BUNCH LENGTH MEASUREMENTS

M. Geitz, Deutsches Elektronen Synchrotron, D-22603 Hamburg, Germany

Abstract

An rf photo-injector in combination with a magnetic bunch compressor is suited to produce high-charged sub-picosecond electron bunches required for electron-drive linacs for VUV and X-ray FELs. This report summarizes time- and frequency domain bunch length measurement techniques with sub-picosecond resolution.

1 INTRODUCTION

Future electron-drive linacs for VUV and X-ray Free Electron Lasers (FEL) require the acceleration of bunches whose length is well in the sub-picosecond regime [1]. A common source for high-charged sub-picosecond electron bunches is an rf gun based on a photo injector using an intense ultraviolet laser beam (typically 20 mJ) to produce up to $5 \cdot 10^{10}$ electrons per bunch from a $CsTe_2$ photo cathode. The electron bunches are accelerated rapidly by the strong electric fields (about 40 MeV/m) of the gun cavity to avoid an emittance blowup due to space charge. The bunch length obtained from an rf gun depends on both the laser pulse length (typically $\sigma_t = 5$ps) and the compression occurring from the rf field within the first centimeters of the gun cavity. By a proper choice of the rf phase a velocity modulation can be impressed on the electron bunch leading to a reduction of its length within the gun cavity. Very short bunches can be obtained at the price of sacrificing a large fraction of the bunch charge. In an electron drive linac only a moderate bunch compression is applied, because of the need of intense electron beams. Further compression can be obtained by combining an off-crest rf acceleration with a magnetic chicane. The off-crest acceleration produces a correlated energy spread with higher energy electrons trailing lower energy electrons. The higher energy electrons then travel on a shorter path through the magnetic chicane than the lower energy electrons and a bunch compression is obtained. In the following an overview of established and future time-domain and frequency-domain bunch length measurement techniques with sub-picosecond resolution will be presented.

2 TIME DOMAIN MEASUREMENTS

Streak Camera: The streak camera is a device for a direct (single-shot) determination of the longitudinal bunch charge distribution. The present resolution limit is 370 fs (FWHM) [2]. The light pulse generated by an

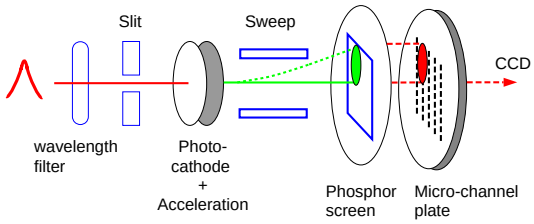

Figure 1: Principle of the streak camera.

electron bunch travels through a dispersion-free optical system, an interference filter and a slit before hitting the photo-cathode of the streak camera. A wavelength filter selects a narrow frequency band and the slit reduces the transverse dimension of the image on the photo cathode. The light pulse is converted to an electron pulse, which is accelerated and swept transversely by a fast rf electric field. The resulting transverse distribution is projected onto a phosphor screen. The image is amplified by a multi-channel plate and then detected by a CCD camera. Space charge effects inside the streak camera tube and the achievable sweeping speed limit the temporal resolution. The energy spread of the electrons generated by the photo-cathode and the dependence of the photo electron energy on the wavelength of the incident light pulse add to the time resolution limit.

A state-of-the-art streak camera measurement performed at the University of Tokyo using a BNL-type rf photo-injector in combination with a magnetic bunch compressor shows a successful compression of a 13 picosecond electron bunch to 440 femtoseconds (FWHM) [3] as shown in Figure 2. The measurement was performed with a bunch charge of 250 pC at an electron energy of 35 MeV.

Rf Kicker Cavity: An interesting proposal to obtain sub-picosecond resolution is the application of the streak camera principle to the electron beam itself [4]. An rf kicker cavity operated in the TM_{110} mode can be used to sweep the electron bunch transversely across a screen located in the vacuum chamber downstream. The transverse

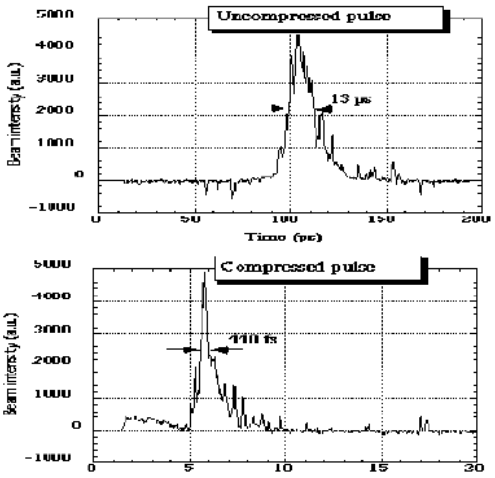

Figure 2: 250 pC electron bunch at 35 MeV beam energy before and after compression with a magnetic chicane compressor at the University of Tokyo [3].

kick k imposed on the bunch with energy E is proportional to

$$k \sim \sqrt{(PQ)} f/E \qquad (1)$$

where P denotes the applied power, f the rf frequency and Q the quality factor of the cavity. It is estimated that a resolution of 100 femtosecond can be realized by either using a high-frequency high-power or high-Q superconducting cavity [4].

Energy Spread Measurements: An efficient and inexpensive way to determine the bunch length is the evaluation of the bunch energy distribution. Figure 4 shows a magnetic bunch compressor chicane followed by an rf cavity and a dispersive section to image the energy profile. The longitudinal dynamics of the system can be described

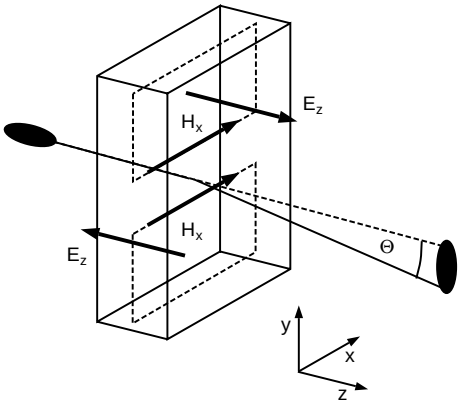

Figure 3: Kicker cavity operated in TM_{110} mode. The bunch is kicked vertically by the magnetic field.

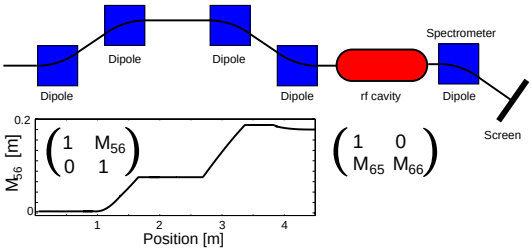

Figure 4: A magnetic bunch compressor chicane followed by an off-crest acceleration can be used to determine the longitudinal bunch charge distribution.

by the transport matrix

$$\left.\begin{pmatrix} L \\ \frac{\Delta E}{E} \end{pmatrix}\right|_{\mathrm{f}} = \begin{pmatrix} 1 & M_{56} \\ M_{65} & M_{56}M_{65} + M_{66} \end{pmatrix} \left.\begin{pmatrix} L \\ \frac{\Delta E}{E} \end{pmatrix}\right|_{\mathrm{i}} \qquad (2)$$

where M_{56}, M_{65} and M_{66} denote transfer matrix elements of the chicane and the rf cavity of Figure 4. If we choose the matrix elements such that $M_{56}M_{65} + M_{66} \rightarrow 0$, the energy profile measured behind the spectrometer dipole magnet is a direct image of the longitudinal bunch charge distribution in front of the compression section [5]. Figure 5 shows energy profile measurements performed at the TESLA Test Facility Linac. With different parameter settings it is possible to measure the longitudinal charge distribution at various positions along the magnetic chicane. The lower plots show the reconstructed compression of the electron bunch

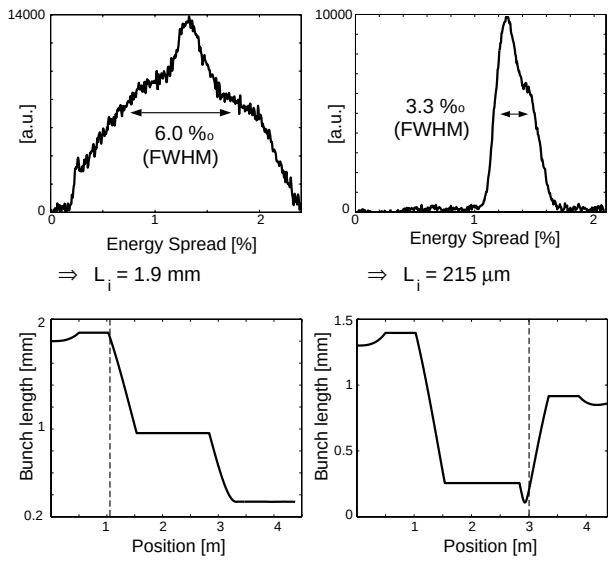

Figure 5: Two energy spread measurements at the end of the TESLA Test Facility Linac. The lower plot shows the reconstructed compression of the bunch length through the chicane compressor. The dashed line shows the longitudinal position where the measured energy profile matches the longitudinal charge distribution. Left: optimum compression. Right: over-compression.

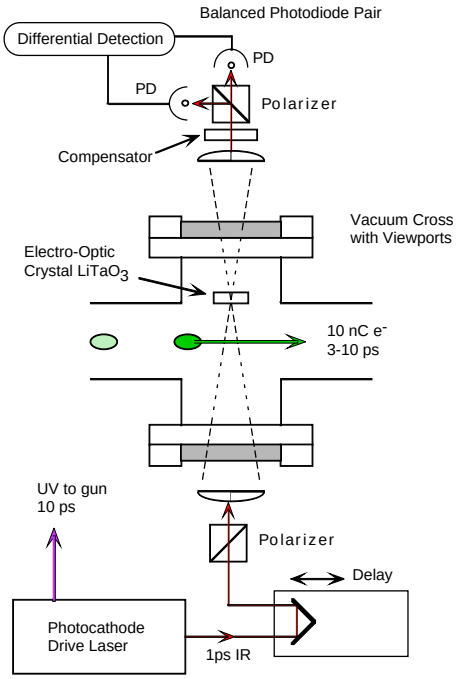

Figure 6: Electro-optic sampling of electric fields carried by the charge distribution by picosecond laser pulses.

within the magnetic chicane. The dashed line indicates the longitudinal position where the energy profile matches the longitudinal charge distribution. This technique is limited by the resolution of the spectrometer and the validity of linear beam transfer. If the bunches become too short, non-linear effects like wake-fields and space charge will have to be taken into account.

Electro-optic Sampling: The principle of electro-optic sampling is to use short laser pulses to probe the change of birefringence in a ZnTe or $LiTaO_3$ crystal introduced by the strong electric fields ($E \approx 3MV/m$) moving with the electron bunch. The laser pulse needed for the photo injector and the electro-optic sampling experiment are produced by the same IR laser to obtain the needed time synchronization. The probe laser beam is delayed by a roof mirror and polarized at 45^o with respect to the axis of ordinary and extra-ordinary refraction of the electro-optic crystal. The imposed elliptical polarization on the probe laser beam is analysed by a polarizing beam splitter and two photo-diodes. By detecting the difference current between the pair of photo-diodes a small modulation depth can be observed. The longitudinal charge distribution is then scanned by delaying the sampling laser pulse with respect to the electron beam [6]. The time resolution is estimated to be in the order of the probe laser pulse length. Electro-optical sampling is a time-domain technique with a large measurement window of about 100 picoseconds (by delaying the sampling laser beam).

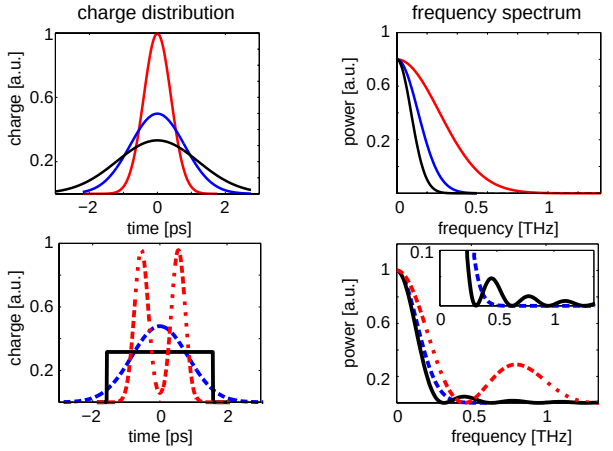

Figure 7: The bunch length and the bunch shape can be distinguished by the obversation of the coherent radiation spectrum. Top: Time- and frequency-domain presentation of three Gaussian bunches of different width. Bottom: Comparison of three bunches of different shape but with equal rms width.

Electro-optic Sampling with Chirped Laser Pulses: The method of electro-optic sampling can be extended to a single-shot measurement by using chirped laser pulses [7] (long wavelengths are leading the short wavelengths). The long laser wavelength samples the beginning, the short laser wavelength the end of the bunch electric fields. The temporal distribution of the electron bunch can be visualized by a diffraction grating viewed by a CCD camera.

3 FREQUENCY DOMAIN MEASUREMENTS

Coherent Transition Radiation (CTR) can be used to determine the longitudinal charge distribution. The radiator is a thin aluminum foil arranged at an angle of 45^o with respect to the beam direction so that the backward lobe of the radiation is emitted at 90^o and is easily extractable from the vacuum chamber. The spectral intensity emitted by a bunch of N particles is

$$I_{\mathrm{tot}}(\omega) = I_1(\omega)\left(N + N(N-1)\left|f(\omega)\right|^2\right) \qquad (3)$$

where $I_1(\omega)$ is the intensity radiated by a single electron at a given frequency ω and $f(\omega)$ is the longitudinal bunch form-factor [8, 9, 10] defined as the Fourier transform of the normalized charge distribution ρ. For a relativistic bunch whose transverse dimensions are small compared to the length the form factor becomes

$$f(\omega) = \int \rho(z)\exp(i\omega z/c)dz = \int c\rho(ct)\exp(i\omega t)dt\ . \qquad (4)$$

For wavelength in the order of the bunch length the form-factor approaches unity. The emitted radiation radiation is then coherent and permits a direct measurement of $|f(\omega)|^2$. Figure 7 shows the expected power spectrum for various bunch length and shapes.

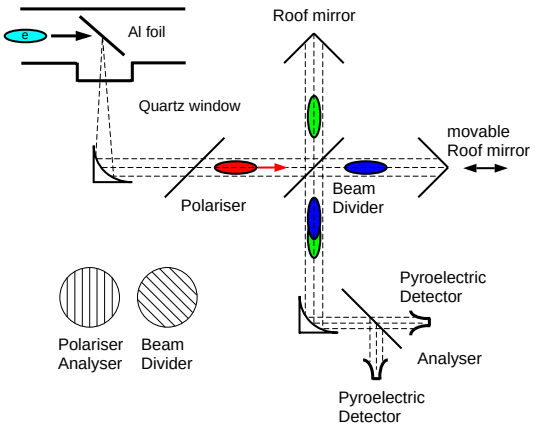

Figure 8: The Martin-Puplett Interferometer.

Fourier Transform Spectroscopy: At the TESLA Test Facility a Martin-Puplett interferometer, shown schematically in Figure 8, has been used to measure the autocorrelation function of the radiation pulse [11]. The diverging transition radiation beam leaving the CTR radiator is transformed into a parallel beam entering the interferometer by a parabolic mirror. The incident radiation pulse is polarized horizontally by the first grid and then splitted by the beam divider into components of different polarization entering the two spectrometer arms. The polarization is flipped by the roof mirrors, hence the component first transmitted at the beam splitter is now reflected and vice versa. The recombined radiation is in general elliptically polarized, depending on the path difference between the two arms. The analyzing grid transmits one polarization component into detector 1 and reflects the orthogonal component into detector 2. Two pyroelectric detectors equipped with horn antennas are used as detection devices for the sub-millimeter wavelength radiation.

A Fourier transformation of the autocorrelation function yields only the absolute magnitude $|f(\omega)|$ of the form factor. A Kramers-Kronig dispersion relation approach can be used to compute the phase of the form factor. The so-called minimal phase ψ is given by [12]

$$\psi(\omega) = \frac{-2\omega}{\pi} \int_0^\infty \frac{\ln[|f(u)|/|f(\omega)|]}{u^2 - \omega^2} du \; . \qquad (5)$$

To carry out the Kramers-Kronig integration a polynomial extrapolation of the form factor towards small frequencies has to be applied [12]. The inverse Fourier transformation then yields the desired longitudinal charge distribution

$$\rho(z) = \int_0^\infty |f(\omega)| \cos\left(\psi(\omega) + \omega z/c\right) d\omega \; . \qquad (6)$$

The steps of the analysis are depicted by the graphs in Figure 9. The drop of the form factor towards small frequencies is explained by a low frequency cut-off of the interferometric device and the acceptance of the pyroelectric detectors. Fourier-transform spectroscopy is a technique with enhanced performance as the bunch length reach the subpicosecond scale. The coherent frequency spectrum then extends well into the THz regime and the high-pass filter effects of the device become less important. Also a greater variety of detecting devices (pyroelectric detectors, Golay-cell detectors, bolometers) is available.

Hilbert Transform Spectroscopy: Hilbert-transform spectroscopy of coherent transition radiation using Josephson junctions offers the possibility for high-speed frequency domain measurements [13, 14, 15]. The electric properties of a junction are determined by Cooper-pair tunneling which leads to the I-U characteristics shown as the dashed curve in Figure 10. A dc current I_0 can be passed through the junction without observing a voltage drop as long as the current stays below a critical value I_c (dc Josephson effect). For currents above I_c a voltage drop across the junction is observed accompanied with an alternating current whose frequency is given by the relation $\omega = 2eU/\hbar$ (ac Josephson effect, $f_{Jos} = \omega/2\pi = 483.6$ GHz for $U = 1$ mV). When the Josephson junction is exposed to monochromatic radiation of (angular) frequency ω the current-voltage characteristic acquires a current step ΔI at the voltage $\overline{U} = (\hbar\omega/2e)$, see Figure 10 ($\overline{U}$ is obtained by averaging over the Josephson oscillation). Within the framework of the Resistively Shunted Junction (RSJ) model [16], and in small-signal approximation, the magnitude of this step is proportional to the power of the incident radiation. Hence the junction acts as a quadratic detector and can be used to measure the spectral intensity of a continuous radiation spectrum. For this purpose we define a

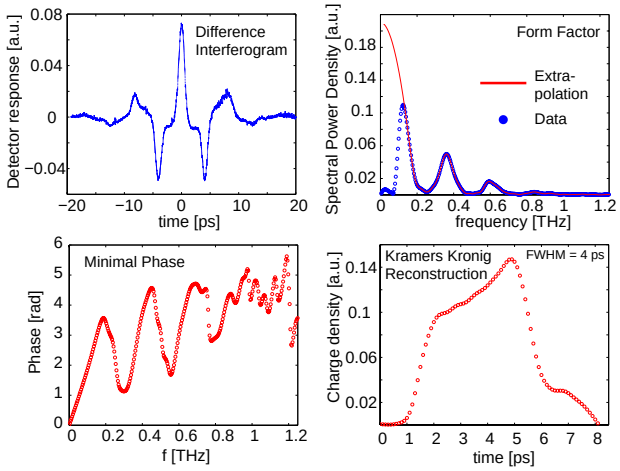

Figure 9: The measured interferogram (upper left) is Fourier-transformed to determine the longitudinal form factor (upper right). The minimal phase is evaluated (lower left) and then used to determine the longitudinal electron charge distribution (lower right) by a Fourier transformation back to time domain.

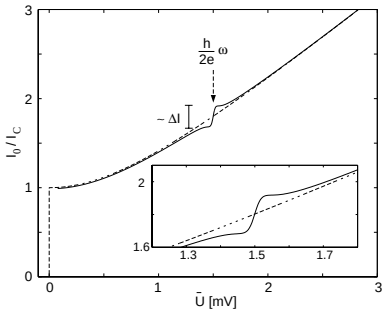

Figure 10: Dashed curve: voltage across the junction as a function of the dc bias current. Solid curve: modification of the dc characteristic curve due to monochromatic incident radiation.

characteristic function

$$g(\overline{U}) = \frac{8}{\pi}\frac{\hbar}{2e}\cdot\frac{\Delta I(\overline{U})I(\overline{U})\overline{U}}{R^2 I_c^2} \qquad (7)$$

where R is the ohmic resistance of the junction. The spectral intensity is derived from g by an inverse Hilbert transform [13]

$$S(\omega) = \frac{1}{\pi}\mathcal{P}\int_{-\infty}^{\infty}\frac{g(\omega_0)\,d\omega_0}{\omega-\omega_0} \quad \text{where} \quad \omega_0 = \frac{2e}{\hbar}\overline{U}\,. \qquad (8)$$

Here $\mathcal{P}$ denotes the principal value of the integral.

Figure 11 shows a coherent power spectrum measured at the TTF linac [15] using a $YBa_2Cu_3O_7$ junction. Also here, the measurement is limited at low frequencies because of the spectral acceptance of the detector. The data are not yet precise enough to derive the bunch shape. Applying a Gaussian fit (solid curve in figure 11) yields $\sigma_t = 1.6$ps. Hilbert-transform spectroscopy is a high-speed technique because of the purely electronic measurement. Using fast read-out electronics (several MHz bandwidth) to sample the I-U curve permits a quick determination of the bunch form factor. Hilbert-transform spectroscopy is limited by the energy gap of the high T_c superconductor that allows for a maximum detectable frequency (generally several THz) before leaving the superconducting state.

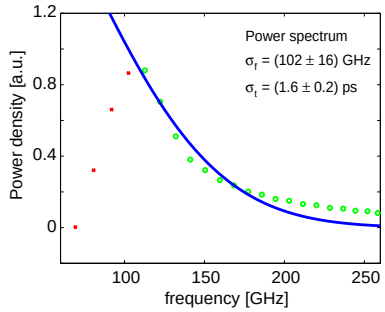

Figure 11: The coherent radiation spectrum as obtained from a discrete Hilbert transform of the characteristic function g. Solid line: Gaussian fit to the power spectrum.

4 CONCLUSION AND OUTLOOK

An rf photo-injector in combination with a magnetic bunch compressor has become a successful instrument for the production of high charged sub-picosecond electron bunches. Bunches as short as σ_t = 240 fs, 250 pC charge at an energy of 35 MeV and σ_t = 10 fs, 20 pC charge at an energy of 70 MeV have been produced. Time-domain measurement techniques are usually applied to single bunches and deliver on-line information of the longitudinal charge distribution. Frequency domain measurement techniques are ideally suited for shorter bunches but have the drawback of longer data acquisition times and rather indirect Fourier analysis methods. The resolution is determined either by the positioning accuracy of the interferometer mirrors and beam-splitter or by the maximum detectable frequency of the Josephson junction determined by Cooper-pair breakup.

5 REFERENCES

[1] TESLA - Collaboration, DESY-TESLA 95-01 (1995).

[2] M. Uesaka et al. , Nucl. Instr. Meth. A 406, (1998), 371 - 379.

[3] M. Uesaka et al. , Proc. of 8^{th} AAC workshop, Baltimore, 1998, to be published.

[4] X. J, Wang, Proc. of PAC Conference, New York, 1999, to be published.

[5] K. N. Ricci et al. , Proc. of FEL Conference, Williamsburg, 1998.

[6] M. J. Fitch et al. , Proc. of PAC Conference, New York, 1999, to be published.

[7] I. Wilke et al. , DESY TTF Report, 1999, to be published.

[8] C. J. Hirschmugl et al. , Phys. Rev. A, Vol. 44, No. 2, (1991).

[9] J. S. Nodvick et al. , Phys. Rev. A, Vol. 96, No. 2, (1954).

[10] E. B. Blum et al. , Nucl. Instr. Meth. A 307, (1991).

[11] B. Leissner et. al. , Proc. of PAC Conference, New York, 1999, to be published.

[12] R. Lai et al. , Nucl. Inst. Meth. A 397, (1997), 221 - 231.

[13] Y. Y. Divin et al. , Appl. Phys. Lett. 68 (11), 1996.

[14] M. Geitz et al., DESY TESLA 98-10, 1998.

[15] M. Geitz et al., Proc. of PAC Conference, New York, 1999, to be published.

[16] K. K. Likharev, Dynamics of Josephson Junctions and Circuits, New York, Gordon Breach, 1996.